Predicting Visible Differences in High Dynamic Range Images - Model and its Calibration

Rafał Mantiuk[a], Scott Daly[b], Karol Myszkowski[a], and Hans-Peter Seidel[a]

[a]MPI Informatik, Stuhlsatzenhausweg 85, 66123 Saarbrücken, Germany;
[b]Sharp Laboratories of America, 5750 NW Pacific Rim Blvd Camas, WA 98607, USA

ABSTRACT

New imaging and rendering systems commonly use physically accurate lighting information in the form of high-dynamic range (HDR) images and video. HDR images contain actual colorimetric or physical values, which can span 14 orders of magnitude, instead of 8-bit renderings, found in standard images. The additional precision and quality retained in HDR visual data is necessary to display images on advanced HDR display devices, capable of showing contrast of 50,000:1, as compared to the contrast of 700:1 for LCD displays. With the development of high-dynamic range visual techniques comes a need for an automatic visual quality assessment of the resulting images.

In this paper we propose several modifications to the Visual Difference Predicator (VDP). The modifications improve the prediction of perceivable differences in the full visible range of luminance and under the adaptation conditions corresponding to real scene observation. The proposed metric takes into account the aspects of high contrast vision, like scattering of the light in the optics (OTF), nonlinear response to light for the full range of luminance, and local adaptation. To calibrate our HDR VDP we perform experiments using an advanced HDR display, capable of displaying the range of luminance that is close to that found in real scenes.

Keywords: Visual difference metric, high dynamic range, HDR, perception, VDP, contrast sensitivity, CSF, OTF, PSF, local adaptation, tvi

1. INTRODUCTION

New imaging and rendering systems commonly use physically accurate lighting information in the form of High-Dynamic Range (HDR) images, textures, environment maps, and light fields in order to capture accurate scene appearance. Unlike their low-dynamic range counterparts, HDR images can contain the entire color gamut and full range of luminance that is visible to a human observer. HDR data can be acquired even with a consumer camera, using multi-exposure techniques,[1] which involve taking several pictures of different exposures and then combining them together into a single HDR image. Another source of HDR data is realistic image synthesis software, which uses physical values of luminance or radiance to represent generated images. Because HDR images can not be directly displayed on conventional LCD or CRT monitors due to their limited luminance range and gamut, methods of luminance compression (tone mapping) and gamut mapping are required.[2–4] Even if traditional monitors cannot accurately display HDR data, new displays of extended contrast and maximum luminance become available.[5] To limit an additional storage overhead for HDR images, efficient encodings formats for HDR images[6–9] and video[10] have been proposed.

When designing an image synthesis or processing application, it is desirable to measure the visual quality of the resulting images. To avoid tedious subjective tests, where a group of people has to assess the quality degradation, objective visual quality metrics can be used. The most successful objective metrics are based on models of the Human Visual System (HVS) and can predict such effects as a non-linear response to luminance, limited sensitivity to spatial and temporal frequencies, and visual masking.[11]

Most of the objective quality metrics have been designed to operate on images or video that is to be displayed on CRT or LCD displays. While this assumption seems to be clearly justified in case of low-dynamic range images,

Further author information: (Send correspondence to R.M.)
R.M.: E-mail: mantiuk@mpi-sb.mpg.de, Telephone: +49 681 9325-427

it poses problems as new applications that operate on HDR data become more common. A perceptual HDR quality metric could be used for the validation of the aforementioned HDR image and video encodings. Another application may involve steering the computation in a realistic image synthesis algorithm, where the amount of computation devoted to a particular region of the scene would depend on the visibility of potential artifacts.

In this paper we propose several modifications to the original Visual Difference Predictor. The modifications improve a prediction of perceivable differences in the full visible range of luminance. This extends the applicability of the original metric from a comparison of displayed images (compressed luminance) to a comparison of real word scenes of measured luminance (HDR images). The proposed metric does not rely on the global state of eye adaptation to luminance, but rather assumes local adaptation to each fragment of a scene. Such local adaptation is essential for a good prediction of contrast visibility in High-Dynamic Range (HDR) images, as a single HDR image can contain both dimly illuminated interior and strong sunlight. For such situations, the assumption of global adaptation to luminance does not hold.

In the following sections we give a brief overview of the objective quality metrics (Section 2), describe our modifications to the VDP (Section 3) and then calibrate the parameters of the proposed metric based on psychophysical data collected in an experiment on a HDR display (Section 4).

2. PREVIOUS WORK

Several visual difference metrics for digital images have been proposed in the literature.[12–19] They vary in complexity and in the visual effects they can predict. However, no metric proposed so far was intended to predict visible differences in High-Dynamic Range images. If a single metric can accurately predict differences for either very dim or bright light conditions, it may fail on images that contain both very dark and very bright areas.

Two of the most popular metrics that are based on models of the HVS are Visual Difference Predictor (VDP)[13] and Sarnoff Visual Discrimination Model.[15] Their predictions were shown to be comparable and the results depended on test images, therefore, on average, both metrics performed equally well.[20] We chose the VDP as a base of our HDR quality metric because of its modularity and thus good extensibility.

In this paper we extend our previous work on HDR VDP.[21] We introduce the influence of the eye optics and we calibrate the VDP parameters for the best prediction of distortions in complex images.

3. VISUAL DIFFERENCE PREDICTOR

In this section we describe our modifications to the original VDP, which enable the prediction of visible differences in HDR images. In this paper we give only a brief overview of the original VDP and focus on the extension to high-dynamic range images. For detailed description of the VDP, refer to.[13]

The data flow diagram of the VDP for high-dynamic range images (HDR VDP) is shown in Figure 1. The HDR VDP receives a pair of images as an input (original and distorted, for example by image compression) and generates a map of probability values, which indicates how likely the differences between those two images are perceived. Both images should be scaled in the units of luminance. In case of low-dynamic range images, pixel values should be inverse gamma corrected and calibrated according to the maximum luminance of the display device. In case of HDR images no such processing is necessary, however luminance should be given in cd/m^2.

The first three stages of HDR VDP model behavior of the optics and retina. The original image is filtered by Optical Transfer Function (OTF), which simulates light scattering in the cornea, lens, and retina. To account for the nonlinear response of photoreceptors to light, the amplitude of the signal is nonlinearly compressed and expressed in the units of Just Noticeable Differences (JND). Because HVS is less sensitive to low and high spatial frequencies, the image is then filtered by Contrast Sensitivity Function (CSF). Those three stages are mostly responsible for contrast reduction in the HVS and are described in detail in the following Sections 3.1, 3.2, and 3.3. The next two computational blocks – the cortex transform and visual masking – decompose the image into spatial and orientational channels and predict perceivable differences in each channel separately. Phase uncertainty further refines the prediction of masking by removing dependence of masking on the phase of the signal. Since the visual masking does not depend on luminance of a stimuli, this part of the VDP is left

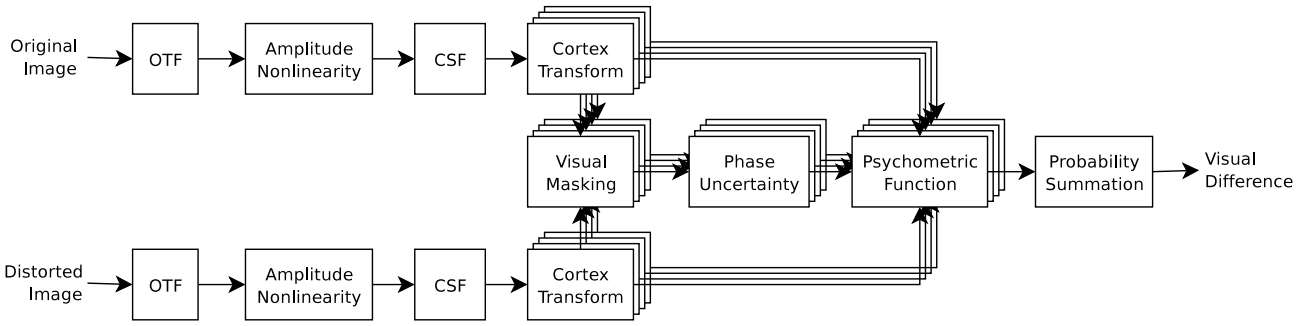

Figure 1. Data flow diagram of the High Dynamic Range Visible Difference Predictor (HDR VDP)

unchanged, except for a minor modification in the normalization of units (details in Section 3.4). In the final error pooling stage the probabilities of visible differences are summed up for all channels and a map of detection probabilities is generated. This step is the same in both versions of the VDP.

3.1. Optical Transfer Function

Due to scattering of light in the cornea, lens and retina, the visibility of low contrast details is significantly reduced in the presence of bright light sources. For example, it is very difficult to see the license plate number at night if the head lamps of the car are on. While such dramatic contrast changes are uncommon for typical LCD for CRT displays, they have significant influence on perception of real life scenes or images seen on HDR displays. To account for this effect, the first stage of HDR VDP simulates light scattering in the human eye for given view conditions.

Light scattering in the optics is usually modeled as Optical Transfer Function (OTF) in the Fourier domain or as Point Spread Function (PSF) in spatial domain. The scattering depends on a number of parameters, such as spatial frequency, wavelength, defocus, pupil size, iris pigmentation, and age of the subject. Because we would like to limit the number of parameters to what is needed for our application, we choose the function of Deeley et al.,[22] which models OTF for monochromatic light and which takes into account luminance adaptation level. The OTF of that model is given by:

$$OTF(\rho, d) = exp[-(\frac{\rho}{20.9 - 2.1d})^{1.3-0.07d}] \tag{1}$$

where d is a pupil diameter in mm and ρ is spatial frequency in cycles per degree. Specifically, the luminance level is taken into account via its effect on the Pupil diameter, calculated for particular adaptation luminance using the formula of Moon and Spencer[23]:

$$d = 4.9 - 3\ tanh\left[0.4\left(\log_{10}(Y_{adapt}) + 1\right)\right] \tag{2}$$

where Y_{adapt} is a global adaptation level in cd/m^2. Figure 2 shows OTFs for several levels of adaptation. The global adaptation level can be calculated as an average luminance of an image in log domain or supplied to the VDP as an external parameter.

3.2. Amplitude Nonlinearity

The original VDP utilizes a model of the photoreceptor to account for non-linear response of HVS to luminance. Perceivable differences in bright regions of a scene would be overestimated without taking into account this non-linearity. The drawback of using the model of the photoreceptor is that it gives arbitrary units of response, which are loosely related to the threshold values of contrast sensitivity studies. The Contrast Sensitivity Function (CSF), which is responsible for the normalization of contrast values to JND units in the original VDP, is scaled in physical units of luminance contrast. Therefore using a physical threshold contrast to normalize response values of the photoreceptor may give an inaccurate estimate of the visibility threshold. Note that the response values are non-linearly related to luminance. Moreover, the model of photoreceptor, which is a sigmoidal response

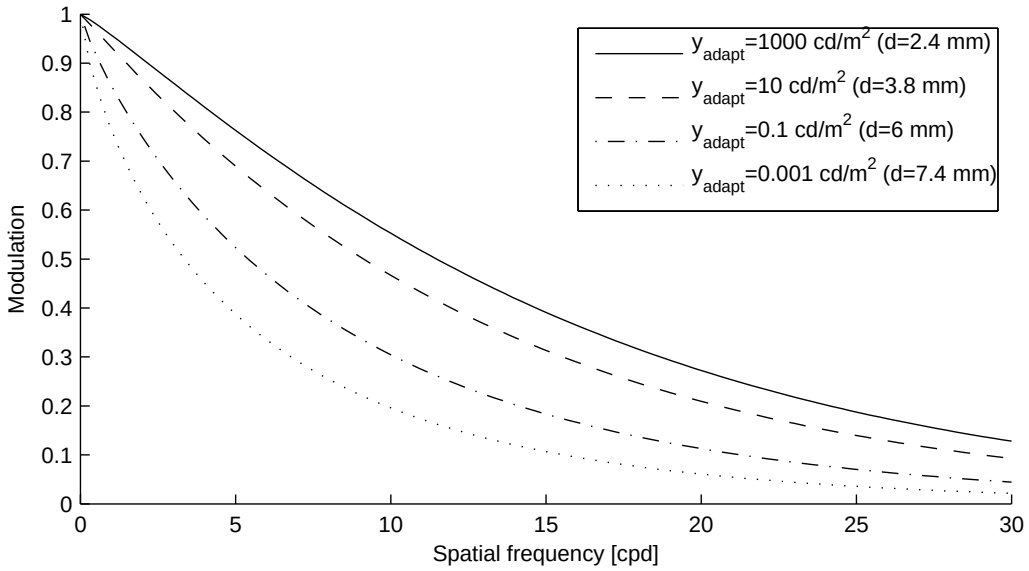

Figure 2. Optical MTFs from the model of Deeley et al.[22] for different levels of adaptation to luminance and pupil diameters (given in parenthesis).

function (see Figure 3), assumes equal loss of sensitivity for low and high luminance levels, while it is known that the loss of sensitivity is generally observed only for low luminance levels* (see Figure 4). Even if the above simplifications are acceptable for low-dynamic range images, they may lead to significant inaccuracies in case of HDR data.

Instead of modeling the photoreceptor response, we propose converting luminance values to a non-linear space that is scaled in JND units.[10, 24] Such space should have the following property: adding or subtracting a value of 1 in this space results in a just perceivable change of relative contrast. To find a proper transformation from luminance to such JND-scaled space, we follow a similar approach as in.[10] Let the threshold contrast be given by the *threshold versus intensity* (*tvi*) function.[25] If $y = \psi(l)$ is a function that converts values in JND-scaled space to luminance, we can rewrite our property as:

$$\psi(l+1) - \psi(l) = tvi(y_{adapt}) \tag{3}$$

where *tvi* is a *threshold versus intensity* function and y_{adapt} is adaptation luminance. A value of the *tvi* function is a minimum difference of luminance that is visible to a human observer. From the first-order Taylor series expansion of the above equation, we get:

$$\frac{d\psi(l)}{dl} = tvi(y_{adapt}) \tag{4}$$

Assuming that the eye can adapt to a single pixel of luminance y as in,[13] that is $y_{adapt} = y = \psi(l)$, the equation can be rewritten as:

$$\frac{d\psi(l)}{dl} = tvi(\psi(l)) \tag{5}$$

*The loss of sensitivity is generally not observed for higher levels of luminance if the eye is adapted to those levels. However, drop of sensitivity can be expected if the eye is adapted to significantly lower luminance than the stimuli. For example there is significant loss of sensitivity for specular highlights in natural images, as the eye is usually adapted to the luminance of an object instead of highlight.

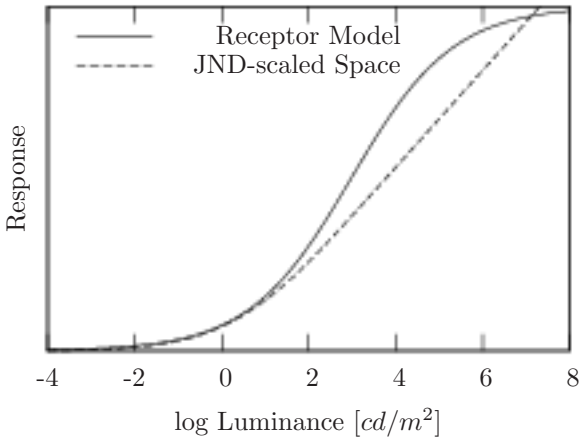

Figure 3. Response curve of the receptor model used in the original VDP (continuous line) and mapping to JND-scaled space used in our HDR extension of the VDP (dashed line). The sigmoidal response of the original receptor model (adaptation to a single pixel) overestimates contrast at luminance levels above 10 cd/m^2 and compresses contrast above $10,000$ cd/m^2. Psychophysical findings do not confirm such luminance compression at high levels of luminance. Another drawback of the receptor model is that the response is not scaled in JND units, so that CSF must be responsible for proper scaling of luminance contrast.

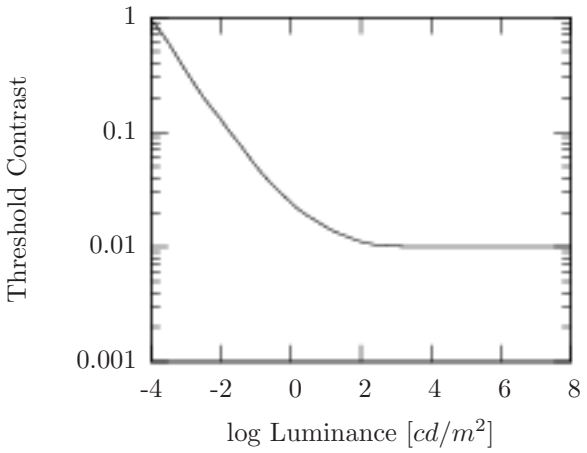

Figure 4. *Contrast versus intensity cvi* function predicts the minimum distinguishable contrast at a particular adaptation level. It is also a conservative estimate of a contrast that introduces a Just Noticeable Difference (JND). The higher values of the *cvi* function at low luminance levels indicate the loss of sensitivity of the human eye for low light conditions. The *cvi* curve shown in this figure was used to derive a function that maps luminance to JND-scaled space.

Finally, the function $\psi(l)$ can be found by solving the above differential equation. In the VDP for HDR images we have to find a value of l for each pixel of luminance y, thus we do not need function ψ, but its inverse ψ^{-1}. This can be easily found since the function ψ is strictly monotonic.

The inverse function $l = \psi^{-1}(y)$ is plotted in Figure 3 together with the original model of photoreceptor. The function properly simulates the loss of sensitivity for scotopic levels of luminance (compare with Figure 4). For the photopic luminance, the function has logarithmic response, which corresponds to Weber's law. A conceptually similar functions were proposed in the literature in the context of tone mapping (*capacity function*)[24] and standardized description of grayscale levels for monitors and hard-copies (*Grayscale Standard Display Function*).[26]

The actual shape of the *threshold versus intensity* (*tvi*) function has been extensively studied and several models have been proposed.[27,28] To be consistent with the original VDP, we derive a *tvi* function from the CSF used there. We find values of the *tvi* function for each adaptation luminance y_{adapt} by looking for the peak sensitivity of the CSF at each y_{adapt}:

$$tvi(y_{adapt}) = P \cdot \frac{y_{adapt}}{max_\rho CSF(\rho, y_{adapt})} \tag{6}$$

where ρ denotes spatial frequency. Similarly as in the the original VDP, parameter P is used to adjust the absolute peak contrast threshold. The optimal value of the parameter P for HDR VDP is calibrated to psychophysical data in Section 4. A function of relative contrast – *contrast versus intensity* ($cvi = tvi/y_{adapt}$) – is often used instead of *tvi* for a better data presentation. The *cvi* function for *tvi* derived by us is plotted in Figure 4.

In our HDR VDP we use a numerical solution of Equation 5 and a binary search on this discrete solution to convert luminance values y to l in JND-scaled space. The subsequent parts of the HDR VDP operate on l values.

3.3. Contrast Sensitivity Function

The Contrast Sensitivity Function (CSF) describes the loss of sensitivity of the eye as a function of spatial frequency and adaptation luminance. It was used in the previous section to derive the *tvi* function. In the original VDP, the CSF is responsible for both modeling the loss of sensitivity and normalizing contrast to JND units. In our HDR VDP, normalization to units of JND at the CSF filtering stage is no longer necessary as the non-linearity step has already scaled the image to JND units (refer to the previous section). Therefore the CSF should predict only the loss of sensitivity for low and high spatial frequencies. The loss of sensitivity in JND-scaled space can be modeled by a CSF that is normalized by peak sensitivity for particular adaptation luminance:

$$CSF_{norm}(\rho, y_{adapt}) = \frac{CSF(\rho, y_{adapt})}{max_{\rho} CSF(\rho, y_{adapt})} \tag{7}$$

Unfortunately, in case of HDR images, a single CSF can not be used for filtering an entire image since the shape of the CSF significantly changes with adaptation luminance. As can be seen in Figure 5, the peak sensitivity shifts from about 2 *cycles/degree* to 7 *cycles/degree* as adaptation luminance changes from scotopic to photopic. To normalize an image by CSF function taking into account different shapes of CSF for different adaptation levels, a separate convolution kernel should be used for each pixel. Because the support of such convolution kernel can be rather large, we use a computationally more effective approach: we filter an image in the Fourier domain several times, each time using CSF for different adaptation luminance. Then, we convert all of the filtered images to the spatial domain and use them to linearly interpolate pixel values. We use luminance values from the original image to determine the adaptation luminance for each pixel (assuming adaptation to a single pixel) and thus to choose filtered images that should be used for interpolation. A more accurate approach would be to compute the adaptation map,[29] which would consider the fact that the eye can not adapt to a single pixel. A similar approach to non-linear filtering, in case of a bilateral filter, was proposed in.[30] The process of filtering using multiple CSFs is shown in Figure 6.

As can be seen in Figure 5, the CSF changes its shape significantly for scotopic and mesopic adaptation luminance and remains constant above $1,000\ cd/m^2$. Therefore it is usually enough to filter the image using a CSF for $y_{adapt} = \{0.0001, 0.01, ..., 1,000\}\ cd/m^2$. The number of filters can be further limited if the image has a lower range of luminance.

CSF predicts the behavior of the complete visual system, including optical and neuronal part. The optical part is however already simulated in HDR VDP pipeline as OTF filtering (see Section 3.1). Therefore, only neural part should play role at this stage of the HDR VDP. To extract neural part from the overall CSF, the CSF can be divided by the OTF.

3.4. Other Modifications

An important difference between the original VDP and the proposed extension for HDR images is that the first one operates on CSF normalized values and the latter one represents channel data in JND-scaled space. Therefore, in case of the VDP for HDR images, original and distorted images can be compared without any additional normalization and scaling. This is possible because a difference between the images that equals one unit in JND-scaled space gives a probability of detection equal to one JND, which is exactly what this step of the VDP assumes. Therefore the contrast difference in the original VDP:

$$\Delta C_{k,l}(i,j) = \frac{B1_{k,l}(i,j)}{\overline{B_K}} - \frac{B2_{k,l}(i,j)}{\overline{B_K}} \tag{8}$$

in case of the VDP for HDR images becomes:

$$\Delta C_{k,l}(i,j) = B1_{k,l}(i,j) - B2_{k,l}(i,j) \tag{9}$$

where k, l are channel indices, i, j pixel coordinates and $B1, B2$ are corresponding contrast values of the channel for the target and mask images.

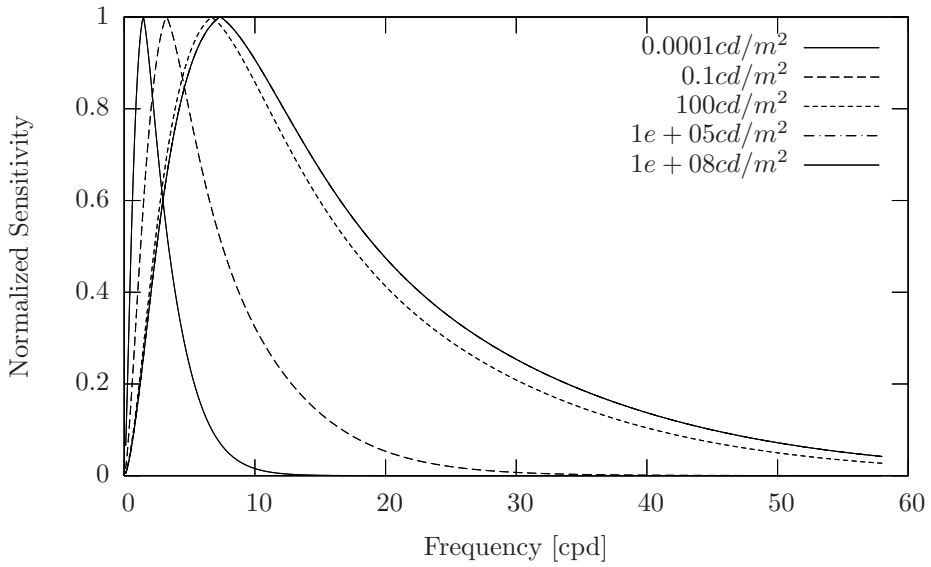

Figure 5. Family of normalized Contrast Sensitivity Functions (CSF) for different adaptation levels. The peak sensitivity shifts towards lower frequencies as the luminance of adaptation decreases. Shape of the CSF does not change significantly for adaptation luminance above 1,000 cd/m^2.

4. CALIBRATION

In our previous work we compared the predictions of the extended HDR VDP with the original VDP.[21] In this work we focus on calibrating HDR VDP for the best prediction of visible differences in complex images. To achieve this we conducted a psychophysical experiment that assessed the detection of differences in complex images. Then we used the collected data to find the best set of HDR VDP parameters that would give its response that is the closest to the result of the subjective tests.

Eight subjects took part in the experiment, which involved detecting visible differences in images shown on a projector based HDR display.[5] The luminance of the HDR images was reproduced on HDR display without any tone compression and was clamped between 0.05 and $2,700 cd/m^2$ (the minimum and maximum luminance that could be achieved on the display). The images were observed from $0.5m$ and each image span about 20 visual degrees. All participants had normal or corrected to normal vision and were experienced in digital imaging.

For each pair of images (original and distorted image), a subject was to mark areas where differences between the images were visible. The marking was done using square blocks of one visual degree edge. Figure 7 shows the screen capture of a testing program. The result of each test was a matrix of 1 and 0 values, where value 1 denoted visible differences in the block and 0 no visible differences. Each subject was to mark eleven image pairs, which contained natural scenes (HDR photographs), computer graphics rendering, and one simple stimuli (luminance ramp). The second image of each pair was distorted with a simple pattern noise, like a narrow band sinusoidal grating, blur, or random noise.

For the data collected from all subjects and for all images, we try to find the best set of HDR VDP parameters, that would give the VDP response, which is the closest to the subjective data. Because the resolution of VDP probability map is one pixel and the resolution of subjective response is a square block of about 30×30 pixels, we have to integrate VDP response, so that the data can be compared (see Figure 8). The natural choice of operator for integration is a maximum probability value (a subject marks the block if any distortion is visible). The VDP probability map however may contain single stray pixels of high probability value, which would cause the high probability of detection for the whole surrounding area. Since it is quite unlikely that a subject will notice the differences in single pixels, we choose percentile, rather than maximum, for integrating over the square block areas. Because we don't know which percentile is the best for integration, we leave it as one of the parameters of the optimization procedure.

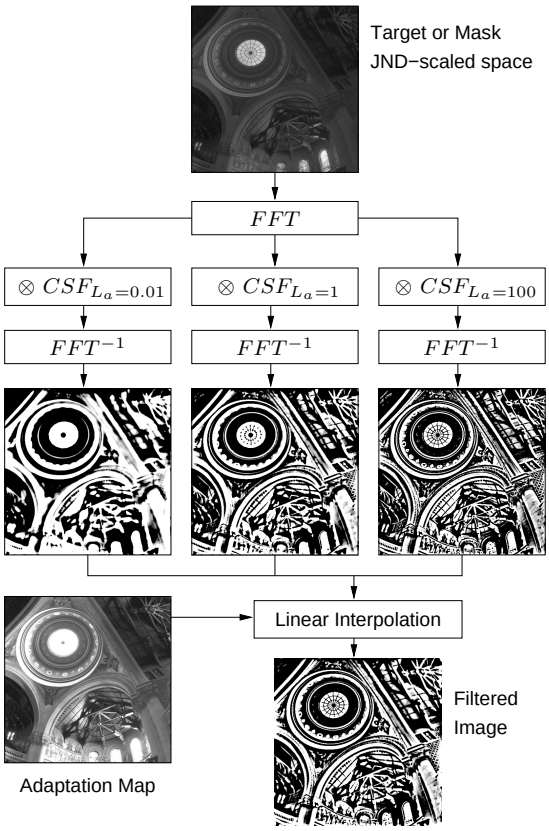

Figure 6. To account for a changing shape of the Contrast Sensitivity Function (CSF) with luminance of adaptation, an image is filtered using several shapes of CSF and then the filtered images are linearly interpolated. The adaptation map is used to decide which pair of filtered images should be chosen for the interpolation.

The fitting function of the optimization procedure has three parameters: a percentile used for integration k, peak contrast sensitivity P, and slope of the masking threshold elevation function s. The peak contrast sensitivity P is the minimum contrast that is visible to a human observer (the inverse of the maximum value of the CSF) and was discussed in Section 3.3. Refer to[13] for the discussion on the slope of the masking function. The fitting function is:

$$f(k,P,s) = \sum_{images} \sum_{blocks} (Int[VDP(p,s),k] - M)^2 \cdot w \tag{10}$$

where the first sum denotes summation over all images, the second over all rectangular blocks, Int is integration over a block using k'th percentile, VDP is the probability map produced by VDP, M is an averaged subjective response and w is the weighting factor for each block. Because for some blocks the visibility of distortions varied for different subjects, the average of subjective response M can contain any value between 0 and 1. For the same reason, the importance of each block is weighted by factor w, which denotes how much trust we can put in subjective data. If some subjects reported distortions in a particular block visible and the other subjects not visible, we can not make solid statement what should be the correct answer. Therefore we use the weighting factor:

$$w = exp(-\frac{D^2}{0.04}) \tag{11}$$

where D is a standard deviation of subjective responses across the subjects. This way the blocks that have standard deviation greater than 0.5 are practically not taken into account in optimization procedure.

We numerically minimalize the fitting function f using several random starting points to find a global minimum. We achieved the best fitting for the parameters: $k = 82$, $P = 0.006$, $s = 1$. The value of 0.6% for the peak

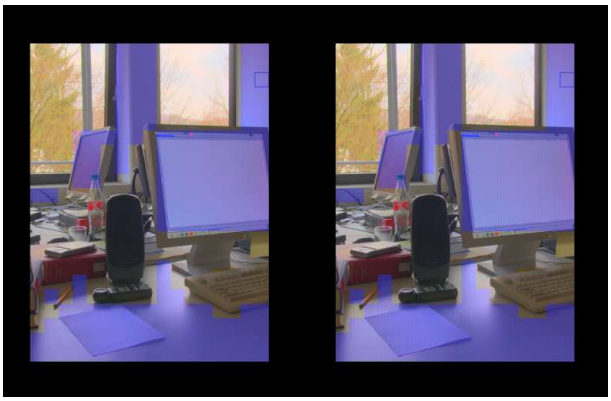

Figure 7. Screen capture of the program used in the experiment. Visible differences between two simultaneously displayed images (original on the left and distorted on the right) were marked with semi-transparent blue square blocks.

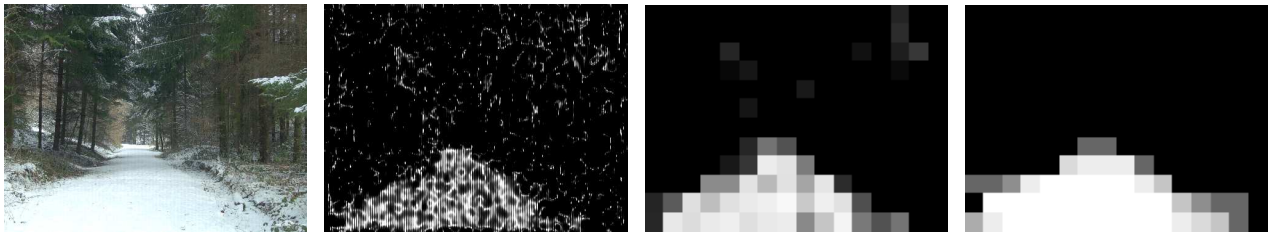

(a) Distorted image (b) VDP prob. map (c) int. prob. map (d) avg subjective resp.

Figure 8. Given the distorted image (a) and its not distorted version, HDR VDP produces a probability map (b). The probability map must be integrated in rectangular blocks (c) before it can be compared with the subjective response (d).

contrast sensitivity P is more conservative than 1% commonly presumed in video and image processing applications, but it also assumes lower sensitivity than the original VDP (0.25%). The slope of the masking threshold elevation function s may vary between 0.65 and 1.0 and can be explained by the learning effect[13] (subjects are more likely to notice differences when the mask is a pattern that is predictable or they are familiar with). Although we let the slope in the optimization procedure be any value in the range of 0.5–1.5, the best fitting was found for the value 1.0, which indicated low learning level. This result was according to our expectations, since complex images form complex masking patterns, which are difficult to learn.

5. CONCLUSION

In this paper we derive several extensions to the original Visual Difference Predictor. The extensions enable the comparison of High-Dynamic Range images. Local contrast reduction is modeled in the extended HDR VDP using three-tier processing: linear shift invariant OTF for light scattering, nonlinear shift invariant conversion to JND-scaled space for the response of the photoreceptor, and the last linear and shift variant CSF for lower sensitivity to low and high spatial frequencies. Such model allows separate processing of high and low contrast information in HDR images. The predictor is then calibrated to the psychophysical data collected in the detection experiment on the HDR display.

In future work we would like to further extend the VDP to handle color images in a similar way as it was done in,[31] but also take into consideration extended color gamut and the influence of chromatic aberration on the OTF.[32] A more extensive validation of HDR VDP predictions is necessary to confirm good correlation between the predicted distortions and the actual quality degradation as perceived by a human observer.

ACKNOWLEDGMENTS

We would like to thank Wolfgang Heidrich for making HDR display available to us and students at the University of British Columbia for participation in the experiment. This work was supported in part by the European Community within the scope of the RealReflect project IST-2001-34744 "Realtime visualization of complex reflectance behavior in virtual prototyping".

REFERENCES

1. M. Robertson, S. Borman, and R. Stevenson, "Dynamic range improvement through multiple exposures," in *Proceedings of the 1999 International Conference on Image Processing (ICIP-99)*, pp. 159–163, (Los Alamitos, CA), Oct. 24–28 1999.
2. K. Devlin, A. Chalmers, A. Wilkie, and W. Purgathofer, "Tone Reproduction and Physically Based Spectral Rendering," in *Eurographics 2002: State of the Art Reports*, pp. 101–123, Eurographics, 2002.
3. F. Drago, W. Martens, K. Myszkowski, and H.-P. Seidel, "Perceptual Evaluation of Tone Mapping Operators with Regard to Similarity and Preference," Technical Report MPI-I-2002-4-002, `http://domino.mpi-sb.mpg.de/internet/reports.nsf/AG4NumberView?OpenView`, Max-Planck-Institut fuer Informatik, Oct. 2002.
4. J. Kuang, H. Yamagishi, G. Johnson, and M. Fairchild, "Testing hdr rendering algorithms," in *IS&T/SID Color Imaging Conference*, pp. 315–320, 2004.
5. H. Seetzen, W. Heidrich, W. Stuerzlinger, G. Ward, L. Whitehead, M. Trentacoste, A. Ghosh, and A. Vorozcovs, "High dynamic range display systems," *ACM Transactions on Graphics* **23**(3), pp. 757–765, 2004.
6. G. Ward, "Real pixels," *Graphics Gems II* , pp. 80–83, 1991.
7. G. Ward Larson, "Logluv encoding for full-gamut, high-dynamic range images," *Journal of Graphics Tools* **3**(1), pp. 815–30, 1998.
8. R. Bogart, F. Kainz, and D. Hess, "OpenEXR image file format," in *ACM SIGGRAPH 2003, Sketches & Applications*, 2003.
9. G. Ward and M. Simmons, "Subband encoding of high dynamic range imagery," in *Proceedings of the 1st Symposium on Applied Perception in Graphics and Visualization*, 2004.
10. R. Mantiuk, G. Krawczyk, K. Myszkowski, and H.-P. Seidel, "Perception-motivated high dynamic range video encoding," *ACM Transactions on Graphics* **23**(3), pp. 730–738, 2004.
11. M. Nadenau, *Integration of Human color vision Models into High Quality Image Compression*. PhD thesis, École Polytechnique Fédéral Lausane, 2000.
12. P. Barten, "Subjective image quality of high-definition television pictures," in *Proc. of the Soc. for Inf. Disp.*, **31**, pp. 239–243, 1990.
13. S. Daly, "The Visible Differences Predictor: An algorithm for the assessment of image fidelity," in *Digital Image and Human Vision*, A. Watson, ed., pp. 179–206, Cambridge, MA: MIT Press, 1993.
14. D. Heeger and P. Teo, "A model of perceptual image fidelity," in *Proc. of IEEE Int'l Conference Image Processing*, pp. 343–345, 1995.
15. J. Lubin, "A visual discrimination model for imaging system design and evaluation," in *Vis. Models for Target Detection*, pp. 245–283, 1995.
16. C. Taylor, Z. Pizlo, J. P. Allebach, and C. Bouman, "Image quality assessment with a Gabor pyramid model of the Human Visual System," in *Hum. Vis. and Elect. Imaging*, pp. 58–69, SPIE Vol. 3016, 1997.
17. Z. Wang and A. Bovik, "A universal image quality index," *IEEE Signal Processing Letters* **9**(3), pp. 81–84, 2002.
18. C. Zetzsche and G. Hauske, "Multiple channel model for the prediction of subjective image quality," in *Human Vision, Visual Processing, and Digital Display*, pp. 209–216, SPIE Vol. 1077, 1989.
19. M. Ramasubramanian, S. N. Pattanaik, and D. P. Greenberg, "A perceptually based physical error metric for realistic image synthesis," in *Proceedings of the 26th annual conference on Computer graphics and interactive techniques*, pp. 73–82, ACM Press/Addison-Wesley Publishing Co., 1999.
20. B. Li, G. Meyer, and R. Klassen, "A comparison of two image quality models," in *Human Vision and Electronic Imaging III*, pp. 98–109, SPIE Vol. 3299, 1998.

21. R. Mantiuk, K. Myszkowski, and H.-P. Seidel, "Visible difference predicator for high dynamic range images," in *Proceedings of IEEE International Conference on Systems, Man and Cybernetics*, pp. 2763–2769, 2004.
22. R. Deeley, N. Drasdo, and W. N. Charman, "A simple parametric model of the human ocular modulation transfer function," *Ophthalmology and Physiological Optics* **11**, pp. 91–93, 1991.
23. P. Moon and D. Spencer, "On the stiles-crawford effect," *J. Opt. Soc. Am.* **34**(319-329), 1944.
24. M. Ashikhmin, "A tone mapping algorithm for high contrast images," in *Rendering Techniques 2002: 13th Eurographics Workshop on Rendering*, pp. 145–156, 2002.
25. D. Hood and M. Finkelstein, "Sensitivity to light," in *Handbook of Perception and Human Performance: 1. Sensory Processes and Perception*, K. Boff, L. Kaufman, and J. Thomas, eds., **1**, Wiley, (New York), 1986.
26. "Part 14: Grayscale standard display function," in *Digital Imaging and Communications in Medicine (DICOM)*, 2001.
27. J. Ferwerda, S. Pattanaik, P. Shirley, and D. Greenberg, "A model of visual adaptation for realistic image synthesis," in *Proceedings of SIGGRAPH 96*, *Computer Graphics Proceedings, Annual Conference Series*, pp. 249–258, Aug. 1996.
28. CIE, *An Analytical Model for Describing the Influence of Lighting Parameters Upon Visual Performance*, vol. 1. Technical Foundations, CIE 19/2.1, International Organization for Standardization, 1981.
29. H. Yee and S. Pattanaik, "Segmentation and adaptive assimilation for detail-preserving display of high-dynamic range images," *The Visual Computer* **19**, pp. 457–466, 2003.
30. F. Durand and J. Dorsey, "Fast bilateral filtering for the display of high-dynamic-range images," in *Proceedings of the 29th annual conference on Computer graphics and interactive techniques*, pp. 257–266, 2002.
31. E. W. Jin, X.-F. Feng, and J. Newell, "The development of a color visual difference model (CVDM)," in *IS&T's 1998 Image Processing, Image Quality, Image Capture, Systems Conf.*, pp. 154–158, 1998.
32. D. Marimont and B. Wandell, "Matching colour images: the effects of axial chromatic aberration," *J. Opt. Soc. Am. A* **11**(12), pp. 2113–3122, 1994.